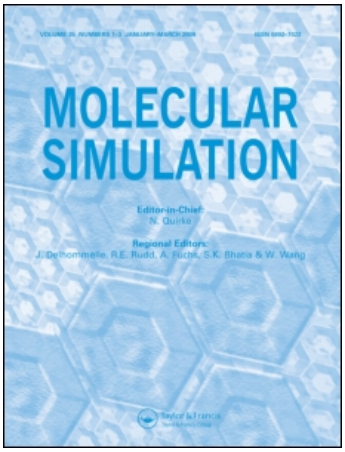

Molecular Simulation
Publication details, including instructions for authors and subscription information:
http://www.informaworld.com/smpp/title~content=t713644482

Phase Diagrams of Diatomic Molecules Using the Gibbs Ensemble Monte Carlo Method

G. Galassi[a]; D. J. Tildesley[a]
[a] Department of Chemistry, The University, Southampton, England

To cite this Article Galassi, G. and Tildesley, D. J.(1994) 'Phase Diagrams of Diatomic Molecules Using the Gibbs Ensemble Monte Carlo Method', Molecular Simulation, 13: 1, 11 — 24
To link to this Article: DOI: 10.1080/08927029408022181
URL: http://dx.doi.org/10.1080/08927029408022181

Molecular Simulation, 1994, Vol. 13, pp. 11–24
Reprints available directly from the publisher
Photocopying permitted by license only

PHASE DIAGRAMS OF DIATOMIC MOLECULES USING THE GIBBS ENSEMBLE MONTE CARLO METHOD

G. GALASSI† and D.J. TILDESLEY

Department of Chemistry, The University, Southampton SO9 5NH, England

(Received July 1993, accepted August 1993)

The Gibbs simulation method is used to explore the phase diagrams of a range of diatomic Lennard-Jones (DLJ) molecules. The dependence of the critical packing fractions on the bond-length of the molecules is examined. Reasonable agreement is found with both experimental and theoretical results. Particular attention is paid to the phase diagram of chlorine and the phase diagram is predicted for a more accurate anisotropic site-site potential. Good agreement is found with the experimental results for both the potential models. We conclude that for chlorine, the liquid-vapour phase envelope is not sensitive to the details of the potential model and therefore cannot be used to improve the model of the intermolecular forces.

1 INTRODUCTION

The Gibbs simulation method [1] is a widely used direct technique for the calculation of phase equilibria (for recent reviews of developments in the field see [2,3]). There have been studies of molecular fluids using models with spherical cores and with additional multipoles [4]. In addition to these there have also been studies of molecular fluids using site-site potentials [5]. In this paper we present results on the phase behaviour of Lennard-Jones diatomics as a function of the bond length. In particular the critical packing fractions and critical temperatures are studied for a variety of homonuclear diatomics and comparison is made with experiment and theory.

Recent work on Cl_2 [6] has demonstrated that by using an anisotropic site-site potential, thermodynamic properties of the crystal, liquid and gaseous phases can be accurately reproduced using the same potential function. In addition the structure factor of the liquid calculated by performing molecular dynamics calculations of the model is in excellent agreement with experiment. Chlorine bas been the subject of previous simulation studies [7,8] and extensive experimental data is also available for the liquid [9]. Neither the DLJ model or this model with additional partial charges to represent the molecular quadrupole, accurately reproduce the liquid structure, although they give a reasonable account of the thermodynamic properties. To investigate the effect of anisotropic interactions on phase coexistence, the phase

† Author for correspondence

diagram of chlorine is calculated with two different potential functions. The first of these is a Lennard-Jones representation of chlorine. This model for chlorine uses an isotropic site-site potential. We have also calculated the phase diagram for chlorine with the anisotropic site-site potential of Rodger *et al.* (the RST potential) [6]. The potential contains anisotropic repulsive, dispersive and electrostatic terms. Of these terms, the anisotropic dispersion is the part of the potential which is most crudely represented. These long range interactions may have a significant effect on the critical point and the locus of the phase coexistence envelope. If the liquid-vapour equilibrium is sensitive to the anisotropy in the dispersion interaction then this part of the potential could be accurately fitted to the coexistence curve. One of the initial aims of this work is to understand the sensitivity of the coexistence curve to the details of the potential.

In section 2 we outline the potentials used in this work. Section 3 describes the details of the Gibbs simulations performed. Section 4 describes the results of the liquid-vapour coexistence of Cl_2 for the DLJ and RST models. Section 5 contains our results for the DI-J potential as a function of elongation and section 6 contains some conclusions.

2 POTENTIALS

The interaction between two molecules depends on the separations of the centres of mass of the two molecules, R_{12} and the three Euler angles θ_1, θ_2 and φ_{12}. The interaction between two molecules can be represented as the sum of four site-site potentials,

$$U(R_{12}, \theta_1, \theta_2, \varphi_{12}) = \sum_{\alpha=1}^{2} \sum_{\gamma=1}^{2} U_{\alpha\gamma}(r_{\alpha\gamma}) \tag{1}$$

where α labels the sites on molecule 1 and γ labels the sites on molecule 2.

In the DLJ potential the site-site potentials are represented by the Lennard-Jones potential,

$$U_{\alpha\gamma}(r_{\alpha\gamma}) = 4\epsilon_{\alpha\gamma}\left[\left(\frac{\sigma_{\alpha\gamma}}{r_{\alpha\gamma}}\right)^{12} - \left(\frac{\sigma_{\alpha\gamma}}{r_{\alpha\gamma}}\right)^{6}\right]. \tag{2}$$

The site-site potential, (2), is isotropic, i.e. it depends only on the separation of the sites and not on the orientation of the site-site vector with respect to the bond vectors of the molecules. To calculate the phase diagram for chlorine using the DLJ potential, it is necessary to know the appropriate values of the parameters $\sigma_{\alpha\gamma}$ and $\epsilon_{\alpha\gamma}$ for the sites and the reduced bond-length for the molecule. In this work, we have used the values of Singer *et al.* [10]. These parameters are,

$$\sigma_{\alpha\gamma} = 3.332\text{Å}$$

$$\epsilon_{\alpha\gamma}/k_B = 178.3\text{K}$$

$$L^* = L/\sigma_{\alpha\gamma} = 0.630$$

where L^* is the reduced bond-length for the molecule. These parameters were obtained by Singer *et al.* as follows. Molecular dynamics simulations were per-

Table 1 The RST potential parameters as defined in eqn (3) [6].

$\sigma_0 = 3.8630$ Å	$\sigma_{110} = 0.0221$ Å	$\sigma_2 = -0.0619$ Å	$\sigma_3 = 0.3500$ Å
$\alpha = 3.5100$ Å^{-1}	$K = 1$ kJ mol^{-1}	$C = 10166.7$ kJ Å^6 mol^{-1}	
$\xi_0 = 0.1629$ Å	$Q_1 = -0.1449$ ea$_0$	$Q_2 = 1.8901$ ea$_0^2$	$l = 1.994$ Å

formed for the diatomic molecule of interest, in this case chlorine. Thermodynamically consistent equations of state were fitted to the simulation data. These equations of state were compared to experimental data along the liquid-vapour coexistence line and the parameters $\sigma_{\alpha\gamma}$ and $\epsilon_{\alpha\gamma}$ adjusted to give the best agreement with the experimental data.

The RST potential by contrast, accurately describes the anisotropies in the various site-site interactions. As such, the potential should give a much more complete description of the interactions between the atoms in chlorine molecules than the Lennard-Jones potential. The RST potential has the form,

$$U_{\alpha\gamma}(r_{\alpha\gamma}) = K\exp[-\alpha(r_{\alpha\gamma}-\sigma_0-\sigma(\Omega))] - C(r_{\alpha\gamma}+\xi_0-\sigma(\Omega))^{-6} + E_{es}$$

$$\sigma(\Omega) = \sigma_{110} + \sigma_2(S_{202}+S_{022}) + \sigma_3(S_{303}+S_{033})$$

$$E_{es} = \frac{1}{4\pi\epsilon_0}[2Q_1^2 S_{112} r_{\alpha\gamma}^{-3} + 3Q_1Q_2(S_{123}+S_{213})r_{\alpha\gamma}^{-4} + 6Q_2^2 S_{224} r_{\alpha\gamma}^{-5}]. \quad (3)$$

In (3), $r_{\alpha\gamma}$ is the intersite separation, K, α, σ_0, C, ξ_0, σ_{110}, σ_2, σ_3, Q_1 and Q_2 are constants whose values are given in table 1. In (3), the term E_{es} represents the electrostatic interaction between the two sites and contains dipole-dipole, dipole-quadrupole and quadrupole-quadrupole interactions. The orientation dependence in the potential comes from the term $\sigma(\Omega)$, which depends on the S functions. The S functions are related to spherical harmonic functions, and are functions of the intersite vector and the vectors pointing along the bonds of the molecules to the interacting sites. The S functions are defined in [6]. The first of the S functions used in (3), S_{202} is,

$$S_{202} = \frac{1}{2}[3(\hat{\mathbf{e}}_\alpha \cdot \hat{\mathbf{r}}_{\alpha\gamma})^2 - 1] \quad (4)$$

where $\hat{\mathbf{e}}_\alpha$ is the unit vector pointing along the bond of the molecule, towards the site α and $\hat{\mathbf{r}}_{\alpha\gamma}$ is the unit vector pointing from site γ on molecule 2 to site α on molecule 1.

3 SIMULATION DETAILS

The phase diagrams for DLJ molecules, with L* = 0.15, 0.30, 0.50, 0.63, 0.75, and 1.00 have been calculated using the Gibbs ensemble method.

The simulations were started from either an α-fcc lattice, or a previously equilibrated configuration. A total of 512 molecules were distributed between the two boxes. Periodic boundary conditions and minimum imaging were applied to the molecular centres, and long range corrections to the pressure and energy calculated for the cutoffs based on centre of mass separations rather than the

separation of the sites. The parameters controlling the maximum allowed volume change of the boxes and the maximum allowed translation and rotation of the molecules were not adjusted during the production phase of the simulations. The number of attempted particle interchanges, was chosen so that a minimum of 2000 successful interchanges occurred during the course of a simulation. In extending the simulation phase diagram for chlorine ($L^* = 0.630$) towards the triple point, it became necessary to implement grid maps [11] to offset the computational cost of the rapid increase in the number of attempted interchanges. Grid maps are an efficient method of detecting attempted particle insertions which create a significant overlap with other particles without recourse to a complete calculation of the trial insertion potential. All the simulations for chlorine below 300K, used grid maps. Typically, close to the critical point, 300 attempted interchanges per cycle were sufficient to equate the chemical potentials in the two regions. However at temperatures closer to the triple point, 15×10^3 attempted interchanges per cycle were required to achieve equilibrium.

A typical simulation at one value of L^* required at least 1000 equilibration cycles followed by 3000 production cycles. A cycle consists of an attempt to alter the positions and orientations of all the molecules in the boxes, one attempted volume change and a number of attempted trial interchanges.

In this paper we also present simulations of the RST potential for chlorine. To calculate the pressure from the RST potential, it is necessary to obtain the analytical derivative of the potential and a method outlined in [121 was used to do so. The angular average of the intermolecular potential [13] and virial were calculated using the NAG routine D0IFCF. The long range corrections were calculated for a range of cutoff distances ranging from 3Å to 50Å, in steps of 0.05Å. The cutoff-correction required for a particular attempted move was obtained from the table by linear interpolation.

The RST potential contains an exponential repulsive term. At small intersite separations the potential becomes attractive. The actual intersite separation at which this occurs at is dependent on the relative orientations of the two molecules. To ensure that this feature of the potential did not cause any difficulties in our simulations, a minimum intersite separation was used, set to 1Å. All site-site interactions at this separation are repulsive, regardless of the orientations of the two molecules. This minimum intersite cutoff was employed in all of the Gibbs simulation moves.

Monte Carlo simulations using the RST potential can become locked in regions of phase space, leading to non-ergodic Markov chains and unreliable averages. Initial Monte Carlo simulations carried out using the RST potential in the constant-NVT ensemble, did not agree with the previous molecular dynamics results [6]. For example, the Monte Carlo simulation at $T = 175$K, $\rho = 0.024459$ mol cm^{-3} was started from an α-fcc lattice with 108 molecules, equilibrated for 6000 cycles and 14000 production cycles performed. A cycle refers to an attempted translation and rotation of all the molecules. The simulation gave a total energy of -20.34 ± 0.11 kJmol^{-1}, the quoted error is calculated by splitting the simulation up into 14 sub-averages and calculating 1 standard deviation in the mean. There appeared to be no significant drift in the energy over the final 5000 cycles of the production period. In contrast, at the same state point, the molecular dynamics results gave an energy of -18.55 ± 0.03 kJmol^{-1}. By running our simulations from equilibrated molecular dynamics configurations, or by heating the systems up to high

reduced temperatures during the equilibration phase of the simulation, agreement was obtained between the two sets of results. For example, a Monte Carlo constant-NVT simulation was performed at $T = 175$K, $\rho = 0.024459$ mol cm^{-3} with 108 molecules. The simulation was started from an α-fcc lattice and equilibrated at $T = 601$K for 2000 cycles. The temperature of the system was gradually annealed down to $T = 175$K over the following 4000 cycles and finally 6000 production cycles were performed. The simulation gave a total energy of -18.56 ± 0.11 kJmol^{-1}, in agreement with the molecular dynamics results.

To avoid this problem in our Gibbs simulations with the RST potential, all the simulations were started from a configuration that had been equilibrated by the annealing constant-NVT method described above. As a check on the accuracy of our results an annealing constant-NVT simulation was carried out for the state on the orthobaric curve at $T = 325$ K and $\rho_{liq} = 0.0182$ mol cm^{-3}. The configurational energy of the liquid phase at this state point in the Gibbs simulation is -15.11 ± 0.29 kJmol^{-1} and the resulting energy from the annealed simulation is -15.06 ± 0.08 kJmol^{-1}. The agreement between the two simulations confirms that the Gibbs simulation had not become trapped in a metastable region.

All the simulations with the RST potential were carried out with 216 molecules distributed between the two boxes.

4 THE PHASE DIAGRAM OF CHLORINE

Table 2 contains the results of our simulations of chlorine at ten different coexistence points. The table compares the experimental coexisting pressures and densities of the two phases [9], with those values calculated using the DU potential. The estimated errors in the table were calculated by dividing the production period of each simulation into 10 batches. The errors quoted in the table represent I standard deviation of the mean of the batch averages.

It is clear from table 2 that the DILJ potential gives coexisting pressures and densities that are in reasonable agreement with the experimental data. Most of the calculated pressures and densities agree with the experimental data to within the error of our data. At temperatures below 240.7K it became difficult to obtain

Table 2 Experimental phase coexistence data and the corresponding DLJ simulation results. The chemical potentials in both phases are equal to within the estimated error.

T/K	ρ_{liq}/mol cm^{-3}		ρ_{vap}/mol cm^{-3}		P_{liq}/MPa	P_{vap}/MPa	
	DLJ	Exp.	DLJ	Exp.	DLJ	DLJ	Exp.
410	0.0129 ± 0.0011	0.0118	0.00383 ± 0.00028	0.00477	7.74 ± 1.66	7.13 ± 0.25	7.18
400	0.0132 ± 0.0006	0.0133	0.00289 ± 0.00026	0.00351	5.26 ± 0.99	5.75 ± 0.39	6.15
375	0.0161 ± 0.0003	0.0155	0.00203 ± 0.00012	0.00197	4.23 ± 1.95	4.31 ± 0.11	4.07
350	0.0173 ± 0.0002	0.0171	0.00122 ± 0.00015	0.00116	2.81 ± 1.21	2.74 ± 0.32	2.57
325	0.0184 ± 0.0002	0.0184	0.00060 ± 0.00009	0.00067	0.94 ± 2.68	1.31 ± 0.22	1.51
300	0.0197 ± 0.0001	0.0195	0.00034 ± 0.00002	0.00036	0.27 ± 1.95	0.79 ± 0.05	0.81
285.2	0.0203 ± 0.00007	0.0202	0.00025 ± 0.00004	0.00024	0.87 ± 1.12	0.54 ± 0.07	0.53
267.4	0.0211 ± 0.00005	0.0209	0.00015 ± 0.00001	0.00014	0.57 ± 1.44	0.32 ± 0.03	0.30
258.5	0.0213 ± 0.00009	0.0212	0.00010 ± 0.00001	0.00010	0.03 ± 1.92	0.22 ± 0.01	0.22
240.7	0.0221 ± 0.0001	0.0219	0.00010 ± 0.00001	0.00005	-0.30 ± 2.15	0.20 ± 0.02	0.10

Table 3 The predicted critical temperatures and densities for the DLJ model of chlorine compared with the experimental values.

β	T_c/K	$\rho_c/mol\ cm^{-3}$	$F_n/10^{-7}$
0.31	419.5	0.00812	0.5625
0.32	420.3	0.00810	0.7758
0.33	422.1	0.00808	6.677
0.34	422.7	0.00807	9.085
0.50	440.9	0.00779	1.069
Expt.	416.95		

sufficient interchanges between the boxes to ensure that the chemical potentials of the two phases are the same and so no results are reported for this region of the coexistence envelope for the DLJ potential.

The critical temperature and density have been calculated for the DLJ potential by fitting the data to the law of rectilinear diameters,

$$\left(\frac{\rho_l + \rho_g}{2}\right) = A(T - T_c) + \rho_c \tag{5}$$

and the appropriate scaling law for the density [14]

$$\rho_l - \rho_g = A|T - T_c|^{\beta}. \tag{6}$$

The experimentally observed scaling exponent, $\beta = 0.32$, has been used in the fitting of the data to the scaling law for the density. In order to obtain an idea of the influence of the scaling exponent on the calculated critical point, a range of other β values have been used in the fitting procedure. The value $\beta = 0.33$ corresponds to the 3D Ising exponent and $\beta = 0.5$ to the mean-field exponent. The critical densities and temperatures calculated using the various values of β are presented in table 3 where they are compared with the experimental values. The value F_n is a measure of the mean-squared deviation of the fit. The critical temperature and density calculated from the Gibbs simulation using $\beta = 0.32$ agree with experiment to within 1%. This is a remarkable result for such a simple potential model. The table demonstrates that the critical exponent used can alter the calculated critical temperature by approximately 29K(7%) and the critical density by approximately 0.000435 mol cm^{-}(5%). In view of the known defects in the potential model the agreement with experiment must be somewhat fortuitous.

In Figure 1 the coexisting densities produced by the DIJ simulations are compared with the experimental results. Included in the figure are the simulation results of Powles [15]. Powles' results were obtained using a method based on the Widom particle insertion technique for the calculation of the chemical potential in the liquid phase and a virial expansion in the vapour phase. The DLJ model for chlorine used by Powles is identical to the model used in this work. Figure 1 spans a significant part of the liquid-vapour coexistence region from the triple point at $T = 172.17$ K to the critical point at $T = 416.96$ K. We are able to use the Gibbs simulation method to investigate temperatures to within 68 K of the triple point where the range of the orthobaric curve is 244 K. We are prevented from going to lower temperatures, even with the use of grid maps, because of the difficulties of obtaining enough accepted exchange moves. The experimental curve shown in Figure 1 was

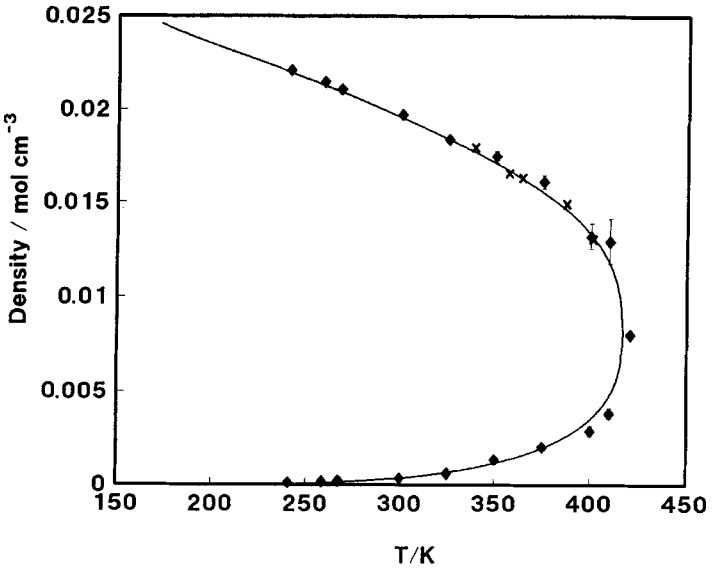

Figure 1 The coexistence curve determined from Gibbs simulations with the DLJ potential. The filled symbols are the Gibb's simulation results, the crosses are the results of Powles [15] and the line is a fit to the experimental data [9].

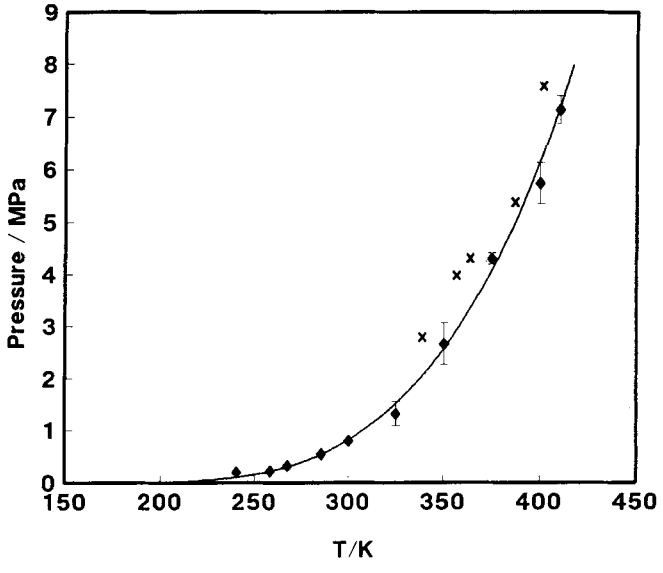

Figure 2 The coexisting vapour pressures from the Gibbs simulation with the DLJ potential. The filled symbols are the Gibbs simulation results, the crosses are the results of Powles [15] and the lines is a fit to the experimental data [9].

calculated from an equation of state obtained by fitting to experimental data obtained from a variety of sources [9] and is of high accuracy. The mean-squared percentage deviation of the simulated liquid densities from the experimental curve is 4.5% whereas the curve fits the measured experimental densities to better than 1%. The results of Powles using the indirect method are in good agreement with Gibbs simulation results and the experiment.

In Figure 2 the coexisting vapour pressures produced by the DLJ simulations are compared with the experimental results and the simulation results of Powles. Once again the experimental curve comes from a critical compilation of the experimental data [9]. The DLJ potential gives a good description of the vapour coexistence pressures in the Gibbs simulation method, but a rather poorer description of the pressures when used in the Powles method. It should be pointed out however that Powles obtained a significantly better fit to the vapour pressures by altering the values of ϵ and σ used in the DLJ potential to,

$$\sigma_{\alpha\gamma} = 3.415\text{Å}$$

$$\epsilon_{\alpha\gamma}/k_B = 185.0\,\text{K}.$$

We did not find that such a scaling of the parameters was necessary.

Simulations of chlorine were also carried out using the RST potential. Table 4 contains the results of our simulations of chlorine at 5 different coexistence points. A comparison of the times required to complete the DLJ and the RST simulations was made at $T = 350\,\text{K}$. Both simulations employed 216 molecules and a cycle consisted of an attempted move for every molecule, 500 attempted exchanges and I attempted volume change per cycle. The calculations were performed on one processor of an Alliant FX80; each cycle for the DLJ potential required 6s of cpu and each cycle for the RST potential required 42.3s. The increase in the required CPU time for the RST potential when is due to the complexity of the functional form of the potential and the extra computation involved in calculating the derivatives of the potential to determine the pressure. The lowest temperature simulation carried out with the RST potential was at a temperature of 300 K. Grid maps were not implemented for the RST potential: the excluded volume of atom is now a complicated function of the intermolecular orientations and it is unlikely that grid-maps will offer a significant advantage. The errors quoted in the table were obtained by the same method as for the DLJ results. The results in Table 4 show that the RST potential gives coexisting pressures and densities that are in reasonable agreement with the experimental data. Critical temperatures and densities have been calculated

Table 4 The experimental phase coexistence data and the corresponding RST simulation results. The chemical potentials in two phases are equal to within the estimated errors.

T/K	$\rho_{liq}/mol\ cm^{-3}$		$\rho_{vap}/mol\ cm^{-3}$		P_{liq}/MPa	P_{vap}/MPa	
	RST	*Exp.*	*RST*	*Exp.*	*RST*	*RST*	*Exp.*
400	0.0137±0.0004	0.0133	0.00394±0.00028	0.00351	7.72±3.73	6.50±0.56	6.15
375	0.0150±0.0007	0.0155	0.00188±0.00031	0.00197	6.55±6.88	4.10±0.45	4.07
350	0.0173±0.0003	0.0171	0.00127±0.00009	0.00116	4.33±3.80	2.89±0.24	2.57
325	0.0182±0.0003	0.0184	0.00060±0.00004	0.00067	−1.06±6.17	1.40±0.11	1.51
300	0.0197±0.0002	0.0195	0.00040±0.00004	0.00036	5.80±6.49	0.90±0.06	0.81

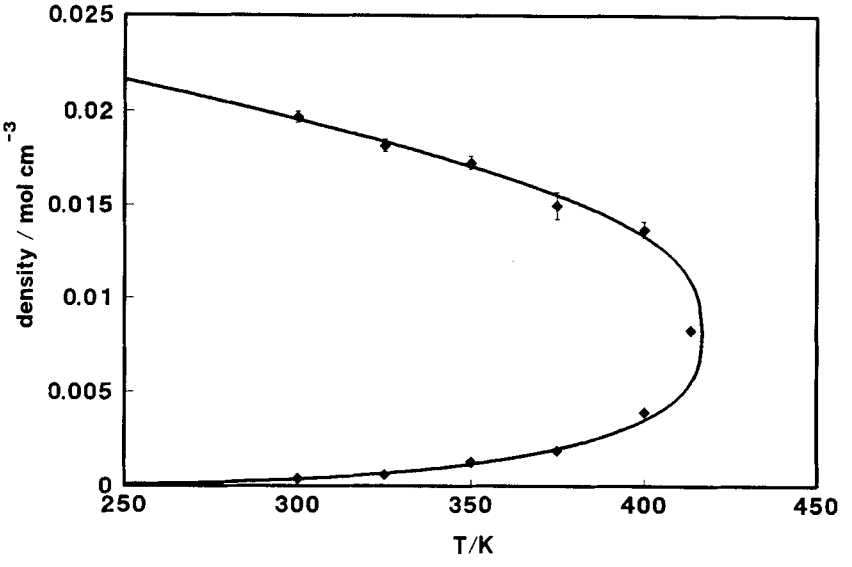

Figure 3 The coexistence curve determined from the Gibbs simulations with the RST potential. The filled symbols are the Gibbs simulation results and the line is a fit to the experimental data [9].

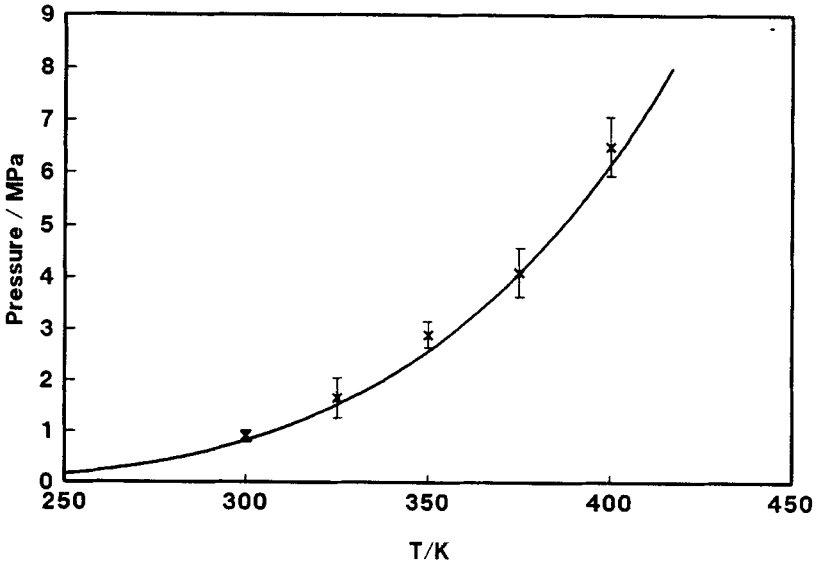

Figure 4 The coexisting vapour pressures from the Gibbs simulation with the RST potential. The filled symbols are the Gibbs simulation results and the line is a fit to the experimental data [9].

Table 5 The critical temperatures and densities for the RST model of chlorine compared with the experimental values.

β	T_c/K	$\rho_c/mol\ cm^{-3}$
0.32	413.38	0.008309
0.50	414.01	0.008301
0.33	390.34	0.008598
Expt.	416.95	0.008134

for the RST potential using the same method as described for the DLJ potential. The critical temperatures and densities calculated using the various values of β are presented in table 5. The critical temperature calculated using the value $\beta = 0.32$ agrees with experiment to within 1% and the density to within 3%.

In Figure 3 the coexisting densities produced by the RST simulations are compared with the experimental results. The RST potential provides a good description of the coexisting densities with most of the densities falling within one error bar of the experimental values.

In Figure 4 the coexisting vapour pressures are presented. Once again most of the simulation results fall within one error bar of the experimental results.

Comparison of the results for the DU and RST models of chlorine shows neither model to be qualitatively superior to the other. Both potential models produce densities and pressures that are in good agreement with the experimental results. The RST potential gives a critical temperature that is below that of the experimental and a critical density that is above the experimentally measured value. The DLJ potential by contrast yields a critical temperature above the experimental value and a critical density below the experimental value.

The agreement between these two different models of chlorine support the view that the liquid-vapour coexistence curve is not sensitive to the details of the potential model for liquid chlorine and this property cannot be used to improve any aspect of the RST potential. Fitting potentials to the coexistence envelope is therefore unlikely to yield better parameters for complicated potential functions and, furthermore, simple potentials which are known to fail in reproducing the liquid structure may do an excellent job at describing the liquid-vapour phase envelope. The atom-atom distribution functions for the RST and DLJ liquids on the orthobaric curve at 300 K are shown in Figure 5. This comparison emphasises that the underlying liquid structure of the RST and DLJ models are quite different. The RST potential produces a second peak in $g_{\alpha\beta}$ which is significantly more pronounced than the corresponding peak for the DU model. The $g_{\alpha\beta}(r_{\alpha\beta})$ of the RST can be Fourier transformed to produce a structure factor which is excellent agreement with experiment [6].

5 RESULTS FOR OTHER DIATOMICS

Gibbs simulations were carried out for a range of DU molecules. The critical densities and temperatures for these molecules were calculated using the same method as described in the previous section.

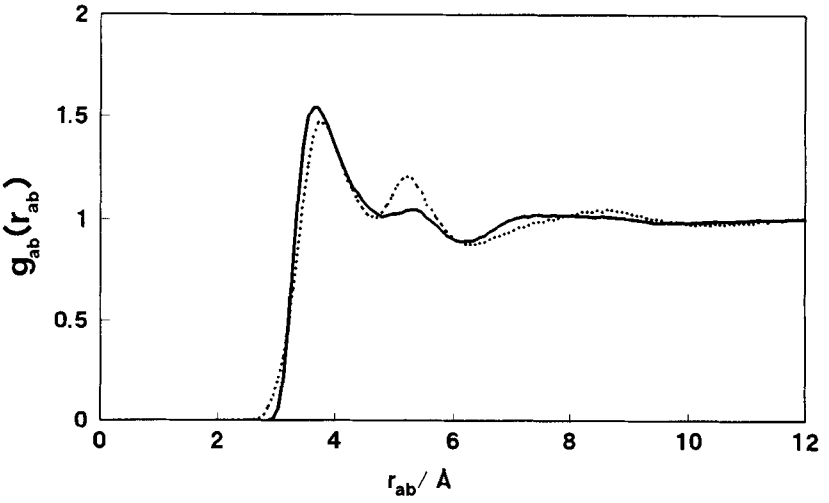

Figure 5 A comparison of the atom-atom radial distribution function for the RST potential (dashed line) and the DLJ potential (solid line) for the liquids on the orthobaric curve at 300 K.

Table 6 Critical points for the Lennard-Jones diatomic fluids.

l^*	T_c^*	ρ_c^*
0.15	4.612	0.2875
0.30	3.640	0.2537
0.50	2.734	0.2061
0.63	2.357	0.1822
0.75	2.099	0.1660
1.00	1.771	0.1441

The critical temperatures and densities calculated for the six diatomics simulated are presented in table 6 and in Figure 6 we present our results for the critical packing fractions as a function of bondlength. The simulation point at the reduced bondlength of 0.0 is taken from Panagiotopoulos [16] and represents the critical point for Lennard-Jones atoms. This critical point was obtained from Gibbs simulations. Also presented in Figure 6 are a number of experimentally measured critical packing fractions and the theoretically predicted results of cluster perturbation theory (CPT) [17]. The experimentally measured critical temperatures and densities [18, 6] and the Lennard-Jones parameters [10, 19, 20] required to put the experimental data into reduced units are presented in table 7. As can be seen from the figure, the simulation results are in good agreement with the experimental results and there is overall agreement with the results of the liquid state theory. The critical densities calculated by CPT are typically within 1 to 3.5% of the experimental results. The critical density from the Gibbs simulation of chlorine using the DLJ potential is within about 0.5% of the experimental results for chlorine and the critical density

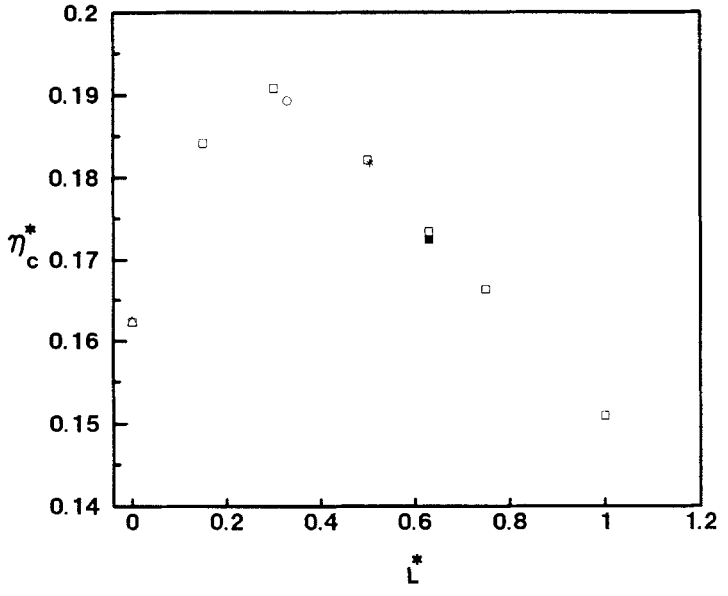

Figure 6 The critical packing fractions as a function of bond-length for the diatomic Lennard-Jones fluid: Gibbs simulation (open squares); *Ar* (open triangle), N_2 (open circle); F_2 (star); Cl_2 (filled square).

Table 7 Critical properties and the appropriate Lennard-Jones parameters for a range of molecules from experiment.

	L^*	$(\epsilon/k_B)/K$	$\sigma/\dot{A}$	T_c^*	ρ_c^*
Ar	0.0	119.8	3.405	1.25	0.318
N_2	0.329	37.30	3.310	3.38	0.245
F_2	0.505	52.8	2.825	2.73	0.205
Cl_2	0.630	178.3	3.332	2.33	0.181

for the simulation of a DLJ molecule with $L^* = 0.500$ is also within 0.5% of the experimentally measured value for fluorine (tables 6 and 7).

The coexistence curves for DU molecules with $L^* = 0.15$, 0.50 and 0.75 are plotted in Figure 7. The curves are plotted in units that are reduced by the critical temperatures and critical packing fractions. The figure illustrates the departure of the molecules from the principle of corresponding states particularly on the liquid side of the phase diagram. The increase in molecular anisotropy with increasing bondlength causes a broadening of the coexistence region. The coexisting gas densities can be scaled onto a universal line by reducing with respect to η_c^* and T_c^*.

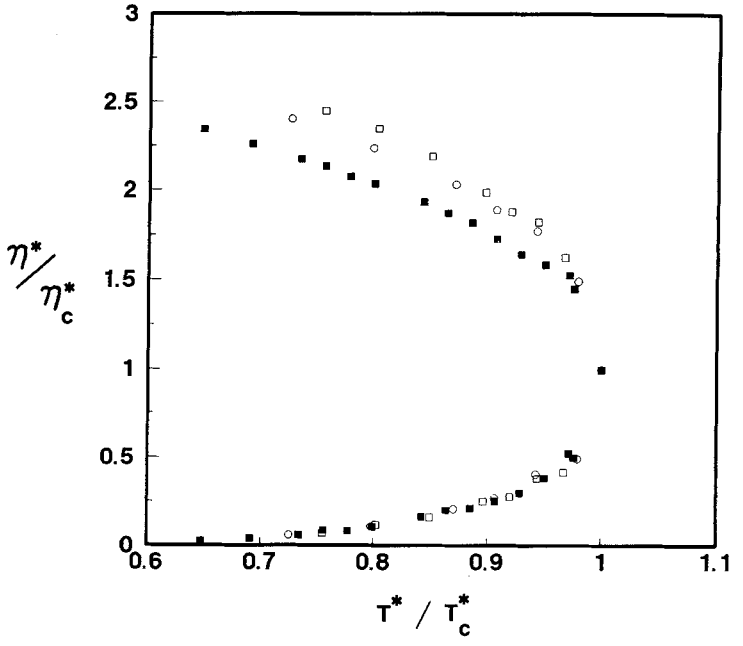

Figure 7 The coexisting packing fractions for DLJ fluids as a function of reduced temperature. The packing fractions and temperatures are reduced by their critical values. $L^* = 0.75$ (open squares); $L^* = 0.50$ (open circles); $L^* = 0.15$ (filled squares).

6 CONCLUSIONS

We have presented simulation results for chlorine, based on two representations of the intermolecular potential. It is established beyond doubt that the RST potential gives an excellent account of the structure of the liquid and solid phases of chlorine. The DLJ potential, which takes no account of the permanent electrostatic interactions between the molecules or the ansisotropy in the repulsion, cannot reproduce either the liquid or solid structures as measured by diffraction. However, both potentials do an excellent job in producing the liquid-vapour coexistence curve and even reproducing the experimental critical points to within a few percent. The positive view of this result is that the Gibbs simulation method is straightforward and accurate method of calculating experimental liquid-vapour and liquid-liquid phase diagrams and that oiily a modest effort will be required to refine potential parameters before the technique can be extended into experimentally difficult regimes. On the negative side, the prediction of the liquid-vapour envelope is not a good test of the details of intermolecular potential and certainly cannot be used to refine the RST potential for Cl_2.

The critical points of a range of DLJ molecules have been investigated by the Gibbs simulation method and good agreement found between the simulation, experimental results and the cluster perturbation theory.

Acknowledgements

We are grateful to Dr. M. Rodger for many helpful discussions concerning the RST potential. DJT would like to thank Professor P. Monson and Professor S.F. O'Shea for many stimulating discussions on this problem during their sabbatical visits to Oxford. G.G. acknowledges the SERC for a studentship and DJT acknowledges support under the CSI grant GR/F/51876.

References

[1] A.Z. Panagiotopoulos, N. Quirke, M.R. Stapleton and D.J. Tildesley, "Phase equilibria by simulation in the Gibbs ensemble. Alternative derivation, generalization and application to mixture and membrane equilibria", *Molec. Phys.*, **63**, 527 (1988).

[2] A.Z. Panagiotopoulos, "Direct determination of fluid phase equilibria by simulation in the Gibbs ensemble: A review", *Molec. Simulation*, **9**, 1 (1992).

[3] B. Smit, *New Perspectives on Computer Simulations in Chemical Physics*, (eds: Allen, M.P. and Tildesley, D.J.), Kjeuver (1993).

[4] M.R. Stapleton, D.J. Tildesley, N. Quirke and A.Z. Panagiotopoulos, "Phase equilibria of quadrupolar fluids by simulation in the Gibbs ensemble", *Molec. Simulation*, **2**, 147 (1989).

[5] J.J. de Pablo and J.M. Prausnitz, "Phase equilibria for fluid mixtures from Monte Carlo simulation", *Fluid Phase Equil.*, **53**, 177 (1989).

[6] P.M. Rodger, A.J Stone and D.J. Tildesley, "The intermolecular potential of chlorine. A three phase study", *Molec. Phys.*, **63**, 173 (1988).

[7] S. Romano and K. Singer, "Calculation of the entropy of liquid chlorine and bromine by computer simulation", *Molec. Phys.*, **37**, 1765 (1979).

[8] M.C. Wojcik, K.E. Gubbins and J.G. Powles, "The thermodynamics of symmetric two centre Lennard-Jones liquids", *Molec. Phys.*, **45**, 1209 (1982).

[9] S. Angus, B. Armstrong and K.M. De Reuck, (editors). *Chlorine, International Thermodynamic Tables Of The Fluid State*, Vol. 8 (Chemical Data Series, No. 31) (Pergamon Press) (1984).

[10] K. Singer, A. Taylor and J.V.L. Singer, "Thermodynamic and structural properties of liquids modelied by '2-Lennard-Jones centres' pair potentials", *Molec. Phys.*, **33**, 1757 (1977).

[11] M.R. Stapleton and A.Z. Panagiotopoulos, "Application of excluded volume map sampling to phase equilibrium calculations in the Gibbs ensemble", *J. Chem. Phys.*, **92**, 1285 (1990).

[12] P.M. Rodger, A.J. Stone and D.J. Tildesley, "Anisotropic site-site potentials in molecular dynamics", *Molec. Simulation.*, **8**, 145 (1992).

[13] J.R. Sweet and W.A. Steele, "Statistical mechanics of linear molecules. I. Potential energy functions", *J. Chem. Phys.*, **47**, 3022 (1969).

[14] J.S. Rowlinson and F.L. Swinton, *Liquids and Liquid Mixtures* (Butterworth Scientific) (1982).

[15] J.G. Powles, "The liquid-vapour coexistence line by computer simulation à la Widom", *Molec. Phys.*, **41**, 715 (1980).

[16] A.Z. Panagiotopoulos, "Direct determination of phase coexistence properties of fluids by Monte Carlo simulation in a new ensemble", *Molec. Phys.*, **61**, 813 (1987).

[17] D.B. McGuigan, M. Lupkowski, D.M. Paquet and P.A. Monson, "Phase-diagrams of interaction site fluids. I. Homonuclear 12-6 diatomics", *Molec. Phys.*, **67**, 33 (1989).

[18] G.W.C. Kaye and T.H. Laby, *Tables of Physical and Chemical Constants and some Mathematical Functions*, (London) (1986).

[19] P.S.Y. Cheung and J.G. Powles, "The properties of liquid nitrogen. IV. A computer simulation", *Molec. Phys.*, **30**, 921 (1975).

[20] G.C. Maitland, M. Rigby, E.B. Smith and W.A. Wakeham, *Intermolecular forces: their origin and determination*, Clarendon Press, Oxford (1981).